

# *The effect of soil moisture perturbations on Indian Monsoon Depressions in a numerical weather prediction model*

Article

Accepted Version

Hunt, K. M. ORCID: <https://orcid.org/0000-0003-1480-3755>  
and Turner, A. G. ORCID: <https://orcid.org/0000-0002-0642-6876> (2017) The effect of soil moisture perturbations on Indian Monsoon Depressions in a numerical weather prediction model. *Journal of Climate*, 30 (21). pp. 8811-8823. ISSN 1520-0442 doi: 10.1175/JCLI-D-16-0733.1 Available at <https://centaur.reading.ac.uk/67424/>

It is advisable to refer to the publisher's version if you intend to cite from the work. See [Guidance on citing](#).

To link to this article DOI: <http://dx.doi.org/10.1175/JCLI-D-16-0733.1>

Publisher: American Meteorological Society

All outputs in CentAUR are protected by Intellectual Property Rights law, including copyright law. Copyright and IPR is retained by the creators or other copyright holders. Terms and conditions for use of this material are defined in the [End User Agreement](#).

[www.reading.ac.uk/centaur](http://www.reading.ac.uk/centaur)

**CentAUR**

Central Archive at the University of Reading

Reading's research outputs online

1    **The Effect of Soil Moisture Perturbations on Indian Monsoon Depressions**  
2    **in a Numerical Weather Prediction Model**

3                    Kieran M. R. Hunt\*

4                    *Department of Meteorology, University of Reading, Reading, United Kingdom.*

4                    Andrew G. Turner

4                    *NCAS-Climate, University of Reading, United Kingdom; and Department of Meteorology,*  
5                    *University of Reading, United Kingdom.*

4    \**Corresponding author address:* Kieran M. R. Hunt, Department of Meteorology, University of  
5    Reading, Reading, UK.

4    E-mail: k.m.r.hunt@reading.ac.uk

## ABSTRACT

4 Indian monsoon depressions (MDs) are synoptic-scale cyclonic systems  
5 that propagate across peninsular India three or four times per monsoon sea-  
6 son. They are responsible for the majority of rainfall in agrarian north India,  
7 thus constraining precipitation estimates is of high importance. Here, we use a  
8 case study from August 2014 to explore the relationship between varying soil  
9 moisture and the resulting track and structure of an incident MD using the Met  
10 Office Unified Model. We use this case study with the view to increasing un-  
11 derstanding of the general impact of soil moisture perturbations on monsoon  
12 depressions. It is found that increasing soil moisture in the monsoon trough  
13 region results in deeper inland penetration and a more developed structure  
14 – e.g. a warmer core in the mid-troposphere and a stronger bimodal potential  
15 vorticity core in the middle/lower troposphere – with more precipitation, and a  
16 structure that in general more closely resembles that found in depressions over  
17 the ocean, indicating that soil moisture may enhance the convective mecha-  
18 nism that drives depressions over land. This experiment also shows that these  
19 changes are most significant when the depression is deep, and negligible when  
20 it is weakening. Increasing soil moisture in the sub-Himalayan *arable zone*,  
21 a region with large irrigation coverage, also caused deeper inland penetration  
22 and some feature enhancement in the upper troposphere but no significant  
23 changes were found in the track heading or lower-tropospheric structure.

## 4 **1. Introduction**

5 Indian monsoon depressions (MDs) are synoptic scale systems that usually originate in the Bay  
6 of Bengal and propagate northwestward across the Indian peninsula, with a mean duration of 4-6  
7 days, and an average frequency of between two and four per summer (Boos et al. 2015; Hunt et al.  
8 2016a). Their spin-up mechanism remains uncertain (Cohen and Boos 2016), although it appears  
9 likely that convective instability of the second kind (CISK; Charney and Eliassen 1964) plays at  
10 least some role (Shukla 1978); however, their primary propagation mechanism has been well de-  
11 scribed, albeit fairly recently (Boos et al. 2015; Hunt and Parker 2016), as a coupling of horizontal  
12 nonlinear advection of the mid-tropospheric potential vorticity maximum and an image vortex in-  
13 teraction of the lower-tropospheric PV maximum with the no-normal flow condition imposed by  
14 the Himalayas.

15 It also remains unclear what synoptic variables, if any, control the duration and ultimate dis-  
16 sipation of MDs; there is some evidence that a contemporaneous monsoon flood year or active  
17 spell tends to extend the duration of depressions in the north of the peninsula (Krishnamurthy and  
18 Shukla 2007; Krishnamurthy and Ajayamohan 2010), although this has not yet been disent-  
19 gled into a primarily synoptic or mesoscale (troposphere or land surface conditions, respectively,  
20 favourable for longer duration) theoretical framework. Nevertheless, recent work has shown that  
21 favourable conditions (e.g. higher vorticity, more moisture) at both scales is correlated with in-  
22 creased MD activity, duration, or intensity: e.g. for soil moisture by Chang et al. (2009); Kishtawal  
23 et al. (2013), and for the active phase of the monsoon by Hunt et al. (2016a).

24 Eltahir (1998) was the first to provide a solid theoretical pathway to accompany the long-held  
25 assertion that an increase in large-scale soil moisture induces enhanced precipitation. He proposed  
26 that the drops in surface albedo and Bowen ratio caused by wetting soil work to increase the near-

27 surface specific moist static energy and boundary layer moist static energy gradient, which results  
28 in more favourable conditions for precipitation. If, however, this is to be an important process in  
29 MDs, it is likely to be indirect (it must also overcome a negative feedback at the MD centre – the  
30 associated lower-tropospheric cold core (Godbole 1977; Hunt et al. 2016a) acts to cool the surface  
31 and increase stability there): the area of maximum precipitation is found to the southwest of the  
32 centre (e.g. Ramanathan and Ramakrishnan 1933) where the (adiabatic) quasigeostrophic omega  
33 equation (e.g. Holton and Hakim 2012) predicts the greatest ascent associated with the balanced  
34 MD vortex will be (Boos et al. 2015); in contrast the Bowen ratio tends to reach a minimum just  
35 ahead (northwest) of the centre (Hunt et al. 2016a). To elucidate this, following Hunt et al. (2016a),  
36 Fig. 1 shows the mean Bowen ratio (ERA-Interim; Dee et al. 2011) and precipitation (TRMM;  
37 Kummerow et al. 1998; Huffman et al. 2010) for a 34-depression composite in which location and  
38 orientation are normalised such that the centre lies at the origin and the heading is up the page;  
39 land-only data were used. As asserted, there is not much spatial similarity between the extrema  
40 of precipitation and Bowen ratio - indicating that if we are to believe previous work suggesting a  
41 link between MD behaviour and underlying soil moisture, it may be a more subtle feedback, or  
42 work on a finer spatial scale, than that suggested by Eltahir (1998). The caveat here is that surface  
43 fluxes are an entirely modelled product in ERA-I, and so have substantial uncertainty; however  
44 this is at least partially addressed by the similarity of composite MD precipitation between ERA-I  
45 and TRMM, and the fact that most rainfall near the centre of a depression is stratiform in nature  
46 (Hunt et al. 2016b). To date, a number of studies have shown that assimilation of soil moisture,  
47 or better initial representation of it, improves the forecast of monsoon depressions in mesoscale  
48 models (Chandrasekar et al. 2007; Vinod Kumar et al. 2007; Chandrasekar et al. 2008; Rajesh  
49 and Pattnaik 2016). Further, it has been shown that inland soil moisture is capable not only of

50 extending the duration of tropical cyclones (Andersen and Shepherd 2017), but in some cases of  
51 allowing them to re-intensify (Kellner et al. 2012).

52 Soil moisture is one of the meteorological variables subject to greatest change with respect to the  
53 progression of the Indian monsoon, largely due to its correlation with accumulated precipitation.  
54 The NOAA CPC reanalysis soil moisture climatology (Van den Dool et al. 2003) and the ESA CCI  
55 satellite-derived soil moisture climatology (Liu et al. 2011, 2012; Wagner et al. 2012) for India for  
56 April, June, August, and September are given in Fig. 2(a) and Fig. 2(b) respectively and show  
57 a clear northwestward advance through most of the season: some areas in the monsoon trough  
58 have September soil moisture more than double that of June. Naïvely, then, we might expect MD  
59 tracks to penetrate deeper inland later into the monsoon season, given the expected influence of  
60 antecedent soil moisture on the development of MDs. Fig. 3 shows the mean MD track for each  
61 month (1979-2015) from the track datasets of Hunt et al. (2016a) and Hurley and Boos (2015)  
62 respectively; note that the MD tracks have been extended to include parts where the depression is  
63 strictly in a monsoon low regime (that is to say, the surface winds are below  $8.5 \text{ m s}^{-1}$ ). There  
64 is some weak evidence here to suggest that not only do MDs tend to progress further inland later  
65 in the season, they also seem more likely to have over-land genesis. This should be taken with  
66 the caveat that large-scale conditions over the subcontinent also clearly play some part, given that  
67 there is evidence that the September tracks start to recede, despite high levels of soil moisture  
68 remaining.

69 So, if soil moisture has some effect on the duration of MDs, which seems at least plausible,  
70 we are then faced with with the secondary question of whether antecedent soil moisture patterns  
71 could affect the heading of existing MDs. Chen et al. (2005) showed that, in theory, the off-  
72 centre latent heat released by the asymmetric rainfall distribution would interact with the local  
73 circulation to create a negative velocity potential southwest of the MD centre, and therefore there

would be some tendency for the MD to move in that direction. However, this mechanism is unlikely to be the primary one, since depressions typically move towards the northwest, rather than the southwest. Furthermore, Baisya et al. (2017) recently showed using a mesoscale model that precipitation intensity in MDs is strongly coupled with antecedent soil moisture. Two simple experiments are therefore proposed: firstly a uniform change in soil moisture across the monsoon trough region to determine the sensitivity of MD duration to antecedent land surface conditions; secondly a uniform change in soil moisture in the highly farmed region across the Himalayan foothills (typically several hundred kilometres north of MD tracks; Roy et al. 2015) to determine to what extent MDs can be steered by soil moisture. These questions are presented in the context of an initial case study, but we hope that the results are sufficiently thought-provoking that further research on this topic will be motivated.

We will discuss the experimental setup and outline the methodology in section 2, then outline and interrogate the results, looking at contrasts in track and structure in section 3 before concluding in section 4.

## **2. The Met Office Unified Model and Experimental Setup**

### *a. Overview and Case Study Selection*

The version of the Met Office Unified Model (hereafter, the UM) used for this study runs the Global Atmosphere 6.0 scheme (GA6.0; Walters et al. 2015) at N768 resolution ( $\sim 26$  km) with 85 vertical levels over a global domain; the numerical scheme is semi-implicit and semi-Lagrangian (Davies et al. 2005), and due to the resolution a number of subgrid processes are parameterised, including convection (e.g. Gregory and Rowntree 1990, with additions).



95 In choosing an appropriate case study to use in this experiment, we were subject to two criteria:  
96 firstly, and more importantly, that the MD happened within the last few years - this means that  
97 higher resolution, better quality analyses are available for initialisation; secondly, that the MD had  
98 a track resembling the average for MDs (see Fig. 3) that it could be seen as a fair representative of  
99 the spectrum of MDs incident on the east coast of the peninsula. The most suitable such event was  
100 the MD of early August 2014, which featured depression-status wind speeds from 200 km south  
101 of Kolkata until it was downgraded to a monsoon low 400 km due south of Delhi. All experiments  
102 were initialised at 00Z on August 3rd, the day this event was declared a monsoon depression.

### 103 *b. The Land Surface Scheme and Parameterisation*

104 The operational land surface model in the Met Office UM is the Joint UK Land Environment  
105 Simulator (JULES; Best et al. 2011). This employs the Met Office Surface Exchanges Scheme  
106 (MOSES; Cox et al. 1999; Essery et al. 2003) to handle hydrological processes both subterranean  
107 and in the boundary layer. A brief description of the governing equations in the soil hydrology  
108 subroutine, which is taken from the relevant part of the MOSES documentation, is given in the  
109 Appendix. The interaction between clouds and shortwave/longwave radiation is also handled ex-  
110 plicitly by the prognostic cloud scheme in the UM (PC2; Wilson et al. 2008) following Edwards  
111 and Slingo (1996).

### 112 *c. Ensemble Generation*

113 There are two types of stochastic perturbation that can be employed to generate a spread of  
114 forecasts in a numerical weather prediction model: uncertainties in the analysis can be represented  
115 by perturbing the initial conditions, whereas uncertainties in the model can be represented by using  
116 any number of physics perturbations (e.g. time-varying parameterisations). Operationally, the Met

117 Office use The Met Office Global and Regional Ensemble Prediction System (MOGREPS; Bowler  
118 et al. 2008) to generate ensemble NWP runs; given that this was designed specifically for the UM,  
119 we aim to make our ensemble generation as similar as possible. MOGREPS uses two distinct  
120 stochastic physics schemes: random parameters (RP) and stochastic kinetic energy backscatter  
121 (SKEB). The former uses the premise that many parameters in the various parameterisations in  
122 the UM are tuned to empirical values that appear to give the best representation of the relevant  
123 process, these can be periodically varied at differing frequencies between physically reasonable  
124 values to produce a spread of forecasts; the latter reintroduces kinetic energy lost through poor  
125 representation of the mechanisms by which small-scale processes cascade energy to larger scales  
126 (Shutts 2005). Initial tests suggested that using SKEB perturbations tended to artificially weaken  
127 MDs and cause them to have much shorter tracks. Thus in our study we used a stochastic perturbed  
128 tendencies (SPT) scheme which simply randomly perturbs the summation of tendencies from all  
129 parameterisations in the model (Buizza et al. 1999).

130 In our ensemble, we must also attempt to represent uncertainties in the analyses that are used  
131 to initialise the model. In MOGREPS this is typically done by applying an ensemble transform  
132 Kalman filter (ETKF; Bishop et al. 2001) to a previous ensemble run, assimilating observations to  
133 assess where perturbations will have the largest impact. As operational ensemble analyses were  
134 not readily available for our case study, we opted to simulate the uncertainty by adding white  
135 noise of amplitude 0.5 K to boundary layer potential temperature. Sensitivity tests determined  
136 that this gave a realistic spread of MD tracks from a short initialisation without suppressing the  
137 development and progression of the depression. For each sub-experiment, which are differentiated  
138 by varying soil moisture in the same region, a ten-member ensemble was used; for each ensemble  
139 member, a random seed was used such that across each experiment each ensemble was generated  
140 via the same set of pseudorandom parameters to allow intercomparability.

#### 141 *d. Soil Moisture Ancillaries*

142 As discussed in the Introduction, two case study experiments are proposed to explore the sen-  
143 sitivity of duration and heading respectively to underlying soil moisture. Fig. 4 shows the masks  
144 used to set up the soil moisture ancillary files: the red polygon covers much of South Asia, the  
145 green polygon covers the typical monsoon trough region, and the orange covers the sub-Himalayan  
146 arable land that is becoming increasingly intensively irrigated and farmed. In each instance, the  
147 soil moisture control (perturbations to which will be used in the experiments) is the August clima-  
148 tology as computed from a fully coupled high-resolution climate simulation in the UM. This was  
149 chosen to reduce spin-up/resolution issues that could be introduced by using a climatology from,  
150 e.g., either of the datasets in Fig. 2. This is the current method used for soil moisture initialisation  
151 of the MetUM in operational NWP mode.

152 For the first experiment (hereafter: *trough zone*), soil moisture in the monsoon trough region  
153 (the green polygon in Fig. 4) - in which MD tracks are typically entirely embedded - was altered  
154 to 1%, 80%, 100% (control), 120%, and 500% of its August climatological value. The 500%  
155 value unsurprisingly gives significant oversaturation across much of the region, where this was  
156 the case, soil moisture values at these locations were set to their saturation values; in reality, this  
157 scaling is achievable only over the dry northwest, and the average saturation value over the trough  
158 region is approximately 167%. Conversely, for the second experiment (hereafter: *arable zone*),  
159 soil moisture over South Asia (the red polygon in Fig. 4) is set to 1% of its August climatological  
160 value, except for inside the arable sub-Himalayan area (orange polygon) where the values were  
161 set to 1%, 50%, 100%, and 500% of the climatology. This region was traced to resemble, as much  
162 as possible, the belt of sub-Himalayan arable grassland where irrigation is becoming rapidly and  
163 increasingly prevalent (Roy et al. 2015) - the area where anthropogenic changes to the surface

are likely to have the biggest impact. Values of soil moisture approaching 1% of the August climatology could be found in an *extremely* dry pre-monsoon period, but we remind the reader that the purpose of this experiment is to test the effect of soil moisture contrast in the region, not necessarily to replicate a physical event.

#### *e. Tracking*

The tracking algorithm used to determine the trajectories of MDs in output data is an updated and extended version of that described in Hunt et al. (2016a). Data at individual timesteps in the output are filtered subject to the IMD criteria for MDs (minimum  $8.5 \text{ m s}^{-1}$  surface wind speed and two closed surface isobars at even hPa values) as well as some transient-filtering criteria (lower-tropospheric vorticity above  $3 \times 10^{-5} \text{ s}^{-1}$ , smoothed MSLP must be local minimum), and single-timepoint candidates are linked together using a simple nearest-neighbour algorithm.

### **3. Results**

#### *a. Tracks*

Tracking results from the *trough zone* experiment are shown in Fig. 5(a). The average tracks for each sub-experiment (thick, coloured lines) were computed using normalised track durations for each of the 10 ensemble members; that is to say points were grouped and averaged by total MD lifetime fraction rather than absolute time since genesis, with termination points for all ensemble members across the experiment given by crosses of the relevant colour. The pale green area underneath is a concave hull of all points of all ensemble tracks from the control sub-experiment (i.e. underlying soil moisture set at 100% of the August climatology). The official IMD track for the event is also given in black for illustration.

185 A first inspection of the average tracks seems to suggest that an increase in underlying antecedent  
 186 soil moisture results in deeper penetration of MDs through the monsoon trough region - this is vis-  
 187 ible both in the average termination points and the individual ones. Further inspection indicates  
 188 that both the 500% and 120%, and 100% and 80% average tracks are closely matched pairs, both  
 189 along track and at termination. The former couple is a result of the August soil climatology already  
 190 being fairly close to saturation in this region, so the difference between 20% extra moisture and  
 191 saturation is fairly small. Performing Hotelling's  $t^2$ -test (Hotelling 1992) – the multidimensional  
 192 generalisation of the standard student's t-test for determining whether data are significantly differ-  
 193 ent from each other (we have also applied Welch's generalisation to allow for unequal variance in  
 194 the two comparison populations (Welch 1947)) – to assess whether the sub-experiment ensemble  
 195 terminations are distinct from each other, we find that all pairs apart from the aforementioned two  
 196 are significantly different from each other at the 95% confidence level. This leads us to conclude  
 197 there is a likely causal relationship between large-scale antecedent soil moisture in the monsoon  
 198 trough region, and the duration/distance travelled by incident monsoon depressions. So, is this  
 199 deeper penetration due to faster inland propagation or a longer duration? Using the ensembles, we  
 200 can compute the mean speeds and durations for the 1%, 80%, 100%, 120%, and 500% ensembles,  
 201 the mean propagation speeds are: 3.7, 3.7, 3.7, 3.9 and 3.9  $\text{m s}^{-1}$  respectively, with corresponding  
 202 mean durations of 3.7, 4.3, 4.4, 4.2, and 4.3 days. Applying a significance test, we find that the  
 203 mean ensemble speeds for the two wettest cases (500% and 120%) are significantly different from  
 204 the drier ones, and that the mean duration for the driest case (1%) is significantly different from  
 205 the four wetter ones.

206 The *arable zone* experiment was set up to determine to what extent moisture changes in relatively  
 207 distant soil could affect the steering of a contemporaneous MD. Recall that for this experiment,  
 208 the soil moisture over South Asia was set to 1% of the climatology, and to the value specified (1%,

209 50%, 100%, or 500%) of the climatology in the sub-Himalayan belt. The results from this exper-  
210 iment are presented in Fig. 5(b) in an identical fashion to those from the *trough zone* experiment.  
211 In the absence of a control run, the concave hull given is for the “100%” ensemble plume. While it  
212 may seem contrived to have such extremely dry soil over almost the entire peninsula for the sake of  
213 establishing a strong contrast for our experiment, these desiccated conditions are not particularly  
214 uncommon in the pre-onset conditions of late May (Fan and van den Dool 2004) where extreme  
215 surface temperatures and scarce precipitation are usual, and depressions can still form in the Bay  
216 of Bengal (Rao and Jayaraman 1958; Mooley 1980).

217 An initial overview of Fig. 5(b) suggests two broad characteristics: firstly, that the spread of en-  
218 semble mean terminations is smaller than in the *trough zone* experiment - this is almost certainly  
219 attributable to the altered soil area both having a smaller area and being further away, and thus  
220 being less influential; secondly, that all the average tracks are shorter than in the previous exper-  
221 iment - plausibly due to a larger area of desiccation than in the 1% *trough zone* sub-experiment  
222 resulting in even less water being available over the peninsula, bearing in mind that MDs draw  
223 moisture in from distances of up to 1000 km (Hunt et al. 2016a). We also note that whilst there is  
224 a perfect rank correlation between soil moisture fractional change and mean termination latitude,  
225 the mean track for the 100% sub-experiment is longer than that for the 500% ensemble. Repeating  
226 the termination point significance analysis carried out for the *trough zone* experiment, we find that  
227 the three wettest sub-experiments have mean track termination points significantly different from  
228 the driest (1%), but not from each other, at a 95% confidence level.

## 229 *b. Structure and evolution*

230 Having established that soil moisture changes, both local and distant, are capable of significantly  
231 altering the track of a passing MD, we will now examine the differing synoptic structure that these

232 changes cause and attempt to bring the discussion to its conclusion. The largest contrast was seen  
233 in the *trough zone* experiment, so we shall start the discussion there. Fig. 6 shows longitude-height  
234 cross-sections through 500%-minus-1% composite variables from the *trough zone* experiment. We  
235 will briefly note here that structural changes of similar shape are found by comparing composites  
236 arising from smaller changes in soil moisture, but with varying losses in magnitude, and hence,  
237 significance. The centre of the MD (assuming one existed) at each timepoint across all ensemble  
238 members for the relevant sub-experiment is centered at the origin; but unlike Fig. 1, we do not  
239 rotate these composites since the soil moisture changes introduced were anisotropic. We note  
240 that these differences are consistent across the other, non-extreme, experiments (not shown) albeit  
241 with reduced areas of significance (typically more confined to the upper troposphere) and smaller  
242 magnitudes.

243 We see that the composite MD for the wettest soil moisture case (in contrast to the driest) is more  
244 intense, as the mid-tropospheric thermal high (Godbole 1977; Hurley and Boos 2015; Hunt et al.  
245 2016a) is markedly stronger, with accompanied strengthening of both the 700 hPa and 500 hPa PV  
246 maxima; secondarily there is evidence of an anomalous west-east circulation with enhanced ascent  
247 ahead of the MD centre (i.e. to the west) with enhanced relative humidity there, and decreased  
248 humidity and PV in the upper troposphere behind the centre; and, further, there is evidence of  
249 increased westward axial tilt with height. We would expect these effects to be associated with  
250 increased precipitation west of the centre, and we see in Fig. 7(a) that this is indeed the case.  
251 Fig. 7 gives the 500%-minus-1% horizontal composite surface precipitation and 850 hPa wind  
252 for both experiments. In the case of the *trough zone* experiment, we see, as expected from the  
253 previous discussion, a substantial increase (beyond  $40 \text{ mm day}^{-1}$ ) in precipitation downshear  
254 (i.e. to the west) of the MD, with some slight reduction towards the east of the centre; however it is  
255 not clear whether the increase in soil moisture enhances precipitation via the Eltahir mechanism,

256 or simply whether it allows more moisture to be inserted into the MD that then grows by other  
257 means. The 850 hPa composite difference winds are also given in this figure; they indicate the  
258 increased soil moisture sets up a large-scale, weak anomalous anti-cyclone that is split roughly  
259 in half, noticeably intensifying the zonal components of the MD circulation near the centre, thus  
260 making the core more cyclonic. This localised feature enhancement of the MD is very similar  
261 to the behaviour over ocean (Hunt et al. 2016a) where features (particularly wind) tend to have  
262 greater magnitude but smaller radial extent.

263 For comparison, the equivalent figure to Fig. 7(a) for the *arable zone* experiment is Fig. 7(b).  
264 Here, the consequence of increased soil moisture is largely confined to the north of the MD as  
265 expected, where a very weak anticyclone is established over the cold high associated with the  
266 wetter ground; although the effect is weaker than in the *trough zone* experiment, there is still an  
267 appreciable increase in the strength of the zonal circulation in the north quadrant of the MD. There  
268 is little change to the precipitation, except for a slight increase in the north over the increased  
269 soil moisture and a reduction in the west. On reflection, we should expect little difference to  
270 the large-scale structure of the MD, but the strongest contrast is likely to be meridional given  
271 the nature of our perturbation; therefore, we now consider some latitude-height cross-sections  
272 for the 500%-minus-1% difference composites. These are given for potential vorticity, relative  
273 humidity, and temperature in Fig. 8. It is clear (and unsurprising) that the effect of changing  
274 *arable zone* soil moisture is felt substantially less by the MD than changing *trough zone* soil  
275 moisture, since the *arable zone* soil moisture perturbation is some distance from the MD core.  
276 The most prominent effect of wetting the soil there is to set up a wet, cool boundary layer; this,  
277 in turn, acts to vertically extend the warm core of the MD while slightly reducing moisture in the  
278 upper troposphere. Computation of mean CAPE (not shown) for each sub-experiment suggests a  
279 slight increase around the centre with increasing soil moisture. There is no real evidence of this



280 apparent strengthening, however, in the precipitation or lower-tropospheric wind fields – the only  
281 appreciable increase in magnitude is of the 700 hPa PV maximum.

282 It is also important to consider how varying soil moisture affects MDs as a function of their  
283 lifetime. For example, one would suppose the impact to be quite minimal while most of the MD  
284 is over the ocean. To test this, we can explore how selected fields from the trough experiment  
285 ensemble sets vary as a function of depression lifetime (simply a normalised time axis: 0% is the  
286 time of MD genesis, 100% is the time of MD lysis) - this is given for four fields in Fig. 9, in  
287 which the colours red, yellow, green, and blue represent fractional changes to trough soil moisture  
288 of 1%, 80%, 120%, and 500% respectively. Each field is computed over a box of side length  
289 250 km centred on the MD centre. The topmost field in the figure is maximum CAPE found in  
290 the quadrant of the aforementioned box that contains the next track point of the MD. There is a  
291 marked region (roughly 40-70% through the MD lifetime) where the average maximum CAPE  
292 in all sub-experiments is significantly higher than during the rest of the lifetime, and it is in this  
293 region that a change in soil moisture has the strongest effect, with the extreme sub-experiments'  
294 ensemble members almost having zero overlap. We also note that here, as well as in the other  
295 fields, predictability is rapidly lost (i.e. the ensemble spread significantly widens) once the MD  
296 starts to dissipate, and further that in this regime the effect of varying soil moisture becomes  
297 negligible. In this particular instance, it is also true that during the spin-up phase of the MD, there  
298 is no obvious correlation between increased soil moisture and enhanced CAPE. The reader's eye  
299 may be drawn to this phase in particular both for its low CAPE and the fact that it continues to  
300 drop in all cases before it hits land. Inspection of contemporaneous reanalyses suggests that this  
301 system existed as a tropical low for a few days in the head of the Bay of Bengal (eroding CAPE),

---

<sup>0</sup>Delineated into NW, NE, SE, and SW; that is, if the MD is propagating WNW, CAPE is computed in the NW quadrant.

302 and – as can be seen from Fig. 5 – remained there for a little longer thereafter (eroding it further,  
303 as seen in Fig. 9).

304 Related to CAPE, but not shown, is convective inhibition (CIN). Changes in soil moisture have  
305 been shown to affect CIN (e.g. Clark and Arritt 1995), which typically reaches minimum mag-  
306 nitude just ahead of the depression centre (Hunt et al. 2016a). Applying the same analysis that  
307 we did for CAPE, we find that in the 1% case, CIN is significantly much more negative (less con-  
308 ducive to convection) and that this extreme is much longer lasting in the vicinity of the centre when  
309 compared to the other cases. The remaining cases did not differ significantly from each other.

310 Second from top in Fig. 9 is the mean total precipitable water in the area surrounding the MD  
311 centre. This field is less variable than CAPE but still displays a clear maximum across all sub-  
312 experiments at approximately 60% of the MD lifetime before rapidly falling away. As with max-  
313 imum CAPE, there is significant correlation between trough soil moisture and mean total precip-  
314 itable water as well as a significant difference between the values of the extreme sub-experiments  
315 during the middle period where the MD is at its strongest, followed by a complete loss of corre-  
316 lation, significance, and predictability after this point; although unlike CAPE, the correlation and  
317 significance are retained during spin-up. Second from bottom is the mean lower/mid-tropospheric  
318 temperature anomaly (averaged 850-400 hPa), here the picture is much the same as for total pre-  
319 cipitable water, although the correlation is no longer significant at the 95% confidence level, and  
320 the ensemble spread does not widen as much during lysis. Finally, at the bottom is maximum  
321 relative vorticity in the lower troposphere (900-800 hPa); whilst this is an inherently variable field,  
322 and consequently although there is arguably some correlation between it and soil moisture during  
323 the period of maximum intensity, it is not significant, nor is the difference between the two ex-  
324 treme sub-experiments significant more than occasionally. That having been said, any semblance  
325 of correlation vanishes, as with the other fields, during the dissipation phase.

## 4. Discussion and conclusion

Monsoon depressions are responsible for the majority of the precipitation incident throughout the summer across northern peninsular India and the monsoon trough region. Previous work has established the possibility of at least a correlative connection between antecedent soil moisture and the behaviour of incident MDs, but this is the first study to investigate the nature of that relationship. Soil moisture, in two key areas where it has previously been identified as variable and of meteorological importance, was varied through multiples of the climatology in a selected NWP case study run in the Met Office Global Unified Model.

We have presented the results of a set of idealised sensitivity tests, each with multiple ensemble members, initialised from the analysis of a typical depression chosen in August 2014. Whilst we have framed these tests in the context of a single MD, significant differences have emerged between the ensembles due to the imposition of soil moisture anomalies; we hope that this will motivate further study of other events to explore the climatological relationship between MDs and soil moisture.

We found that both the structure and propagation of the MD was significantly sensitive to changes in soil moisture in the monsoon trough region: wetter conditions there caused a strengthening of the MD with increased central PV and a warmer thermal core, as well as a more pronounced westward axial tilt. Such cases were also found to travel further inland before dissipating. Further, we found that these changes were greatest (among variables associated with MD strength: CAPE, TPW, mid-tropospheric temperature, and lower-tropospheric vorticity) during the period when the MD is most intense, and that varying soil moisture has no noticeable effect on the MD during its spin-down.

348 In the other experiment, soil across South Asia was kept desiccated while moisture in the sub-  
349 Himalayan *arable zone* was varied. This had a lesser effect on both the structure and track of the  
350 case study, although some significant differences persisted: tracks in the wetter cases terminated  
351 later, and there was some weak strengthening of the MD in the middle and upper troposphere.

352 We also noted that in the wetter *trough zone* experiments, the ensemble composite MD became  
353 more axially confined (as well as more intense), mimicking MD behaviour over the ocean (Hunt  
354 et al. 2016a). This suggests that added soil moisture in this region provides more moisture to the  
355 lower troposphere and subsequently enhances convective activity related to the MD. This is further  
356 enhanced by increased lower-level convergence to the west of the centre.

357 This leaves us with several questions for further study. Firstly, how exactly does a monsoon  
358 depression interact with the boundary layer? It has been indicated both here and in previous  
359 work that MDs are very efficient at moving water from the surface through the PBL and into the  
360 troposphere, despite not having particularly high wind speeds (by definition MDs lie at between 5  
361 and 7 on the Beaufort Scale). This could be appropriately investigated by examination of a case  
362 study in a mesoscale-resolution NWP model. Secondly, how would an incident MD respond to  
363 horizontal gradients in soil moisture, rather than the block changes performed in this study; for  
364 example with increasing (and decreasing) values both along track and across track? Thirdly, even  
365 though we have spoken of CISK as the energy source for MDs, the precise role of CISK, and  
366 its magnitude, remains uncertain. Uncovering the true MD spin-up mechanism would provide  
367 invaluable direction for future research on the topic, and could be investigated using mechanism-  
368 denial experiments in a suitable NWP framework (cf. Craig and Gray 1996).

369 *Acknowledgments.* KMRH received partial support from the Met Office under the aegis of the  
370 NERC CASE studentship scheme, and was also supported by the NERC grant NE/L501608/1.

371 KMRH wishes to thank Paul Earnshaw and David Walters at the Met Office for their untiring  
372 assistance with setting up the UM.

373 KMRH also wishes to thank Christopher Taylor at CEH for helpful discussions regarding soil  
374 moisture.

375 A G Turner was supported by the INCOMPASS project (NERC grant number NE/L01386X/1).

## 376 APPENDIX

### 377 A1. Overview of the land surface scheme used in the model

378 Four soil layers are used, for both the thermodynamic and hydrological subroutines, at depths  
379 from the surface of 10, 25, 65, and 200 cm respectively; the prognostic total soil water in each  
380 layer is given by:

$$M = \rho_w \Delta z \Theta_u \quad (\text{A1})$$

381 where  $\rho_w$  is the density of water,  $\Delta z$  is the thickness of the layer, and  $\Theta_u$  is the liquid water  
382 concentration (for the sake of this discussion, we neglect frozen water, although it is catered for in  
383 the scheme). This is subject to the transport equation:

$$\frac{dM_n}{dt} = W_{n-1} - W_n - E_n, \quad (\text{A2})$$

384 where subscript  $n$  denotes the layer,  $W_n$  and  $W_{n-1}$  the diffusion terms in the layer and that immedi-  
385 ately below it, and  $E_n$  is the evapotranspiration (including interaction with roots). The evapotran-  
386 spiration function is controlled by land usage and vegetation data embedded in JULES, whereas  
387 the diffusion terms are prescribed by the Darcy equation:

$$W = K \left( \frac{\partial \Psi}{\partial z} + 1 \right), \quad (\text{A3})$$

where  $K$  is the hydraulic conductivity and  $\Psi$  is the soil water suction function. Within MOSES these are respectively described by the Clapp-Hornberger relationships (Clapp and Hornberger 1978):

$$\Psi = \Psi_s S_u^{-b} \quad (\text{A4})$$

$$K = K_s S_u^{2b+3}, \quad (\text{A5})$$

where  $\Psi_s$ ,  $K_s$  and  $b$  are empirical constants that can be set on model initialisation. For this study, the default values used operationally by the Met Office were used.

There are then two boundary conditions: at the surface, the flux (aside from evaporation) is computed as the summation of canopy throughfall, snowmelt, and surface runoff; underneath the bottom (Nth) layer, the drainage ( $W_N$ ) is set to equal the hydraulic conductivity.

Finally, the evaporation to the atmosphere from soil at the surface is given by:

$$E = \rho C_H U_1 [q_{\text{sat}}(T_\star, p_\star) - q_1] \left[ f_a + (1 - f_a) \frac{g_s}{g_s + C_H U_1} \right] \quad (\text{A6})$$

where  $f_a$  is the tile saturation fraction (e.g. 1 for ice, lake, ocean, 0 for dry rock),  $\rho$  is the density of air,  $g_s$  is the surface soil conductivity,  $U$  is the wind speed,  $C_H$  is the surface flux heat exchange coefficient,  $q$  is specific humidity; and the subscripts  $\star$ , 1, and sat refer to the surface, lowest atmospheric model level, and saturation respectively.

## References

- Andersen, T., and M. Shepherd, 2017: Inland tropical cyclones and the “brown ocean concept. *Hurricanes and Climate Change*, Springer, 117–134.
- Baisya, H., S. Pattnaik, and P. V. Rajesh, 2017: Land surface-precipitation feedback analysis for a landfalling monsoon depression in the Indian region. *J. Adv. Model Earth Sy.*, accepted.

- Best, M. J., and Coauthors, 2011: The Joint UK Land Environment Simulator (JULES), model description—Part 1: energy and water fluxes. *Geosci. Model Dev.*, **4** (3), 677–699, doi:10.5194/gmd-4-677-2011, URL <http://www.geosci-model-dev.net/4/677/2011/>.
- Bishop, C. H., B. J. Etherton, and S. J. Majumdar, 2001: Adaptive sampling with the ensemble transform Kalman filter. Part I: Theoretical aspects. *Mon. Wea. Rev.*, **129** (3), 420–436, doi:10.1175/1520-0493(2001)129<0420:ASWTET>2.0.CO;2, URL [http://dx.doi.org/10.1175/1520-0493\(2001\)129<0420:ASWTET>2.0.CO;2](http://dx.doi.org/10.1175/1520-0493(2001)129<0420:ASWTET>2.0.CO;2).
- Boos, W. R., J. V. Hurley, and V. S. Murthy, 2015: Adiabatic westward drift of Indian monsoon depressions. *Quart. J. Roy. Meteor. Soc.*, **141**, 1035–1048, doi:10.1002/qj.2454, URL <http://dx.doi.org/10.1002/qj.2454>.
- Bowler, N. E., A. Arribas, K. R. Mylne, K. B. Robertson, and S. E. Beare, 2008: The MOGREPS short-range ensemble prediction system. *Quart. J. Roy. Meteor. Soc.*, **134** (632), 703–722, doi:10.1002/qj.234, URL <http://dx.doi.org/10.1002/qj.234>.
- Buizza, R., M. Milleer, and T. N. Palmer, 1999: Stochastic representation of model uncertainties in the ECMWF ensemble prediction system. *Quart. J. Roy. Meteor. Soc.*, **125** (560), 2887–2908, doi:10.1002/qj.49712556006, URL <http://dx.doi.org/10.1002/qj.49712556006>.
- Chandrasekar, A., K. Alapaty, and D. S. Niyogi, 2007: The effect of a surface data assimilation technique and the traditional four-dimensional data assimilation on the simulation of a monsoon depression over India using a mesoscale model. *Nat. Hazards*, **42** (2), 439–453, doi:10.1007/s11069-006-9080-3, URL <http://dx.doi.org/10.1007/s11069-006-9080-3>.
- Chandrasekar, A., K. Alapaty, and D. S. Niyogi, 2008: The impacts of indirect soil moisture assimilation and direct surface temperature and humidity assimilation on a mesoscale model

simulation of an Indian monsoon depression. *J. Appl. Meteor. Climatol.*, **47** (5), 1393–1412,  
doi:10.1175/2007JAMC1599.1, URL <http://dx.doi.org/10.1175/2007JAMC1599.1>.

Chang, H. I., D. Niyogi, A. Kumar, C. M. Kishtawal, J. Dudhia, F. Chen, U. C. Mohanty, and  
M. Shepherd, 2009: Possible relation between land surface feedback and the post-landfall  
structure of monsoon depressions. *Geophys. Res. Lett.*, **36**, doi:10.1029/2009GL037781, URL  
<http://dx.doi.org/10.1029/2009GL037781>.

Charney, J. G., and A. Eliassen, 1964: On the growth of the hurricane depression. *J. Atmos. Sci.*,  
**21** (1), 68–75, doi:10.1175/1520-0469(1964)021<0068:OTGOTH>2.0.CO;2, URL [http://dx.doi.org/10.1175/1520-0469\(1964\)021<0068:OTGOTH>2.0.CO;2](http://dx.doi.org/10.1175/1520-0469(1964)021<0068:OTGOTH>2.0.CO;2).

Chen, T.-C., J.-H. Yoon, and S.-Y. Wang, 2005: Westward propagation of the Indian monsoon  
depression. *Tellus*, **57A**, 758–769, doi:10.1111/j.1600-0870.2005.00140.x, URL <http://dx.doi.org/10.1111/j.1600-0870.2005.00140.x>.

Clapp, R. B., and G. M. Hornberger, 1978: Empirical equations for some soil hydraulic properties.  
*Water Resour. Res.*, **14** (4), 601–604, doi:10.1029/WR014i004p00601, URL <http://dx.doi.org/10.1029/WR014i004p00601>.

Clark, C. A., and R. W. Arritt, 1995: Numerical simulations of the effect of soil moisture and  
vegetation cover on the development of deep convection. *J. Appl. Meteor.*, **34** (9), 2029–2045.

Cohen, N. Y., and W. R. Boos, 2016: Perspectives on moist baroclinic instability: implications  
for the growth of monsoon depressions. *J. Atmos. Sci.*, **73** (4), 1767–1788, doi:  
10.1175/JAS-D-15-0254.1, URL <http://dx.doi.org/10.1175/JAS-D-15-0254.1>.

Cox, P. M., R. A. Betts, C. B. Bunton, R. L. H. Essery, P. R. Rowntree, and J. Smith, 1999: The  
impact of new land surface physics on the gcm simulation of climate and climate sensitivity.



451 *Climate Dyn.*, **15** (3), 183–203, doi:10.1007/s003820050276, URL [http://dx.doi.org/10.1007/](http://dx.doi.org/10.1007/s003820050276)  
452 [s003820050276](http://dx.doi.org/10.1007/s003820050276).

453 Craig, G. C., and S. L. Gray, 1996: CISK or WISHE as the mechanism for tropical cyclone  
454 intensification. *J. Atmos. Sci.*, **53** (23), 3528–3540, doi:10.1175/1520-0469(1996)053<3528:  
455 COWATM>2.0.CO;2, URL [http://dx.doi.org/10.1175/1520-0469\(1996\)053<3528:COWATM>2.](http://dx.doi.org/10.1175/1520-0469(1996)053<3528:COWATM>2.0.CO;2)  
456 [0.CO;2](http://dx.doi.org/10.1175/1520-0469(1996)053<3528:COWATM>2.0.CO;2).

457 Davies, T., M. J. P. Cullen, A. J. Malcolm, M. H. Mawson, A. Staniforth, A. A. White, and  
458 N. Wood, 2005: A new dynamical core for the Met Office’s global and regional modelling  
459 of the atmosphere. *Quart. J. Roy. Meteor. Soc.*, **131** (608), 1759–1782, doi:10.1256/qj.04.101,  
460 URL <http://dx.doi.org/10.1256/qj.04.101>.

461 Dee, D. P., and Coauthors, 2011: The ERA-Interim reanalysis: configuration and performance of  
462 the data assimilation system. *Quart. J. Roy. Meteor. Soc.*, **137** (656), 553–597, doi:10.1002/qj.  
463 828, URL <http://dx.doi.org/10.1002/qj.828>.

464 Edwards, J. M., and A. Slingo, 1996: Studies with a flexible new radiation code. I: Choosing a  
465 configuration for a large-scale model. *Quart. J. Roy. Meteor. Soc.*, **122**, 689–719.

466 Eltahir, E. A. B., 1998: A soil moisture–rainfall feedback mechanism: 1. Theory and observations.  
467 *Water Resour. Res.*, **34** (4), 765–776, doi:10.1029/97WR03499, URL [http://dx.doi.org/10.1029/](http://dx.doi.org/10.1029/97WR03499)  
468 [97WR03499](http://dx.doi.org/10.1029/97WR03499).

469 Essery, R. L. H., M. J. Best, R. A. Betts, P. M. Cox, and C. M. Taylor, 2003: Explicit representation  
470 of subgrid heterogeneity in a GCM land surface scheme. *J. Hydrometeor.*, **4** (3), 530–543, doi:  
471 [10.1029/97WR03499](http://dx.doi.org/10.1029/97WR03499), URL <http://dx.doi.org/10.1029/97WR03499>.

472 Fan, Y., and H. van den Dool, 2004: Climate Prediction Center global monthly soil moisture  
 473 data set at 0.5 degree resolution for 1948 to present. *J. Geophys. Res. Atmos.*, **109** (D10), doi:  
 474 10.1029/2003JD004345, URL <http://dx.doi.org/10.1029/2003JD004345>.

475 Godbole, R. V., 1977: The composite structure of the monsoon depression. *Tellus*, **29**,  
 476 25–40, doi:10.1111/j.2153-3490.1977.tb00706.x, URL [http://dx.doi.org/10.1111/j.2153-3490.](http://dx.doi.org/10.1111/j.2153-3490.1977.tb00706.x)  
 477 1977.tb00706.x.

478 Gregory, D., and P. R. Rowntree, 1990: A mass flux convection scheme with representation of  
 479 cloud ensemble characteristics and stability-dependent closure. *Mon. Wea. Rev.*, **118** (7), 1483–  
 480 1506, doi:10.1175/1520-0493(1990)118<1483:AMFCSW>2.0.CO;2, URL [http://dx.doi.org/10.](http://dx.doi.org/10.1175/1520-0493(1990)118<1483:AMFCSW>2.0.CO;2)  
 481 1175/1520-0493(1990)118<1483:AMFCSW>2.0.CO;2.

482 Holton, J. R., and G. J. Hakim, 2012: *An introduction to dynamic meteorology*, Vol. 88. Academic  
 483 press.

484 Hotelling, H., 1992: The generalization of Student's ratio. *Breakthroughs in Statis-*  
 485 *tics*, Springer, 54–65, doi:10.1007/978-1-4612-0919-5\_4, URL [http://dx.doi.org/10.1007/](http://dx.doi.org/10.1007/978-1-4612-0919-5_4)  
 486 978-1-4612-0919-5\_4.

487 Huffman, G. J., R. F. Adler, D. T. Bolvin, and E. J. Nelkin, 2010: The TRMM multi-satellite  
 488 precipitation analysis (TMPA). *Satellite rainfall applications for surface hydrology*, Springer,  
 489 3–22, doi:10.1007/978-90-481-2915-7\_1, URL [http://dx.doi.org/10.1007/978-90-481-2915-7\\_](http://dx.doi.org/10.1007/978-90-481-2915-7_1)  
 490 1.

491 Hunt, K. M. R., and D. J. Parker, 2016: The movement of Indian monsoon depressions by inter-  
 492 action with image vortices near the Himalayan wall. *Quart. J. Roy. Meteor. Soc.*, **142** (698A),  
 493 2224–2229, doi:10.1002/qj.2812, URL <http://dx.doi.org/10.1002/qj.2812>.

494 Hunt, K. M. R., A. G. Turner, P. M. Inness, D. E. Parker, and R. C. Levine, 2016a: On the  
 495 structure and dynamics of Indian monsoon depressions. *Mon. Wea. Rev.*, **144** (9), 3391–3416,  
 496 doi:10.1175/MWR-D-15-0138.1, URL <http://dx.doi.org/10.1175/MWR-D-15-0138.1>.

497 Hunt, K. M. R., A. G. Turner, and D. E. Parker, 2016b: The spatiotemporal structure of precip-  
 498 itation in Indian monsoon depressions. *Quart. J. Roy. Meteor. Soc.*, doi:10.1002/qj.2901, URL  
 499 <http://dx.doi.org/10.1002/qj.2901>, in press.

500 Hurley, J. V., and W. R. Boos, 2015: A global climatology of monsoon low pressure systems.  
 501 *Quart. J. Roy. Meteor. Soc.*, **141**, 1049–1064, doi:10.1002/qj.2447, URL [http://dx.doi.org/10.](http://dx.doi.org/10.1002/qj.2447)  
 502 [1002/qj.2447](http://dx.doi.org/10.1002/qj.2447).

503 Kellner, O., D. Niyogi, M. Lei, and A. Kumar, 2012: The role of anomalous soil moisture on the  
 504 inland reintensification of Tropical Storm Erin (2007). *Natural Hazards*, **63** (3), 1573–1600.

505 Kishtawal, C., D. Niyogi, B. Rajagopalan, M. Rajeevan, N. Jaiswal, and U. Mohanty, 2013:  
 506 Enhancement of inland penetration of monsoon depressions in the Bay of Bengal due to  
 507 prestorm ground wetness. *Water Resour. Res.*, **49** (6), 3589–3600, doi:10.1002/wrcr.20301,  
 508 URL <http://dx.doi.org/10.1002/wrcr.20301>.

509 Krishnamurthy, V., and R. S. Ajayamohan, 2010: Composite structure of monsoon low pres-  
 510 sure systems and its relation to Indian rainfall. *J. Climate*, **23**, 4285–4305, doi:10.1175/  
 511 [2010JCLI2953.1](http://dx.doi.org/10.1175/2010JCLI2953.1), URL <http://dx.doi.org/10.1175/2010JCLI2953.1>.

512 Krishnamurthy, V., and J. Shukla, 2007: Intraseasonal and seasonally persisting patterns of In-  
 513 dian monsoon rainfall. *J. Climate*, **20**, 3–20, doi:10.1175/JCLI3981.1, URL [http://dx.doi.org/](http://dx.doi.org/10.1175/JCLI3981.1)  
 514 [10.1175/JCLI3981.1](http://dx.doi.org/10.1175/JCLI3981.1).

515 Kummerow, C., W. Barnes, T. Kozu, J. Shiue, and J. Simpson, 1998: The Tropical Rain-  
 516 fall Measuring Mission (TRMM) sensor package. *J. Atmos. Oceanic Technol.*, **15**, 809–817,  
 517 doi:10.1175/1520-0426(1998)015<0809:TTRMMT>2.0.CO;2, URL [http://dx.doi.org/10.1175/](http://dx.doi.org/10.1175/1520-0426(1998)015<0809:TTRMMT>2.0.CO;2)  
 518 1520-0426(1998)015<0809:TTRMMT>2.0.CO;2.

519 Liu, Y.-Y., W. A. Dorigo, R. M. Parinussa, R. A. M. de Jeu, W. Wagner, M. F. McCabe, J. P. Evans,  
 520 and A. I. J. M. Van Dijk, 2012: Trend-preserving blending of passive and active microwave  
 521 soil moisture retrievals. *Remote Sens. Env.*, **123**, 280–297, doi:10.1016/j.rse.2012.03.014, URL  
 522 <http://dx.doi.org/10.1016/j.rse.2012.03.014>.

523 Liu, Y.-Y., R. Parinussa, W. A. Dorigo, R. A. M. De Jeu, W. Wagner, A. I. J. M. Van Dijk, M. F.  
 524 McCabe, and J. P. Evans, 2011: Developing an improved soil moisture dataset by blending pas-  
 525 sive and active microwave satellite-based retrievals. *Hydrol. Earth Syst. Sci.*, **15** (2), 425–436,  
 526 doi:doi:10.5194/hess-15-425-2011, URL <http://www.hydrol-earth-syst-sci.net/15/425/2011>.

527 Mooley, D. A., 1980: Severe cyclonic storms in the Bay of Bengal, 1877-1977. *Mon. Wea. Rev.*,  
 528 **108** (10), 1647–1655, doi:10.1175/1520-0493(1980)108<1647:SCSITB>2.0.CO;2, URL [http://dx.doi.org/10.1175/1520-0493\(1980\)108<1647:SCSITB>2.0.CO;2](http://dx.doi.org/10.1175/1520-0493(1980)108<1647:SCSITB>2.0.CO;2).

530 Rajesh, P. V., and S. Pattnaik, 2016: High resolution land surface response of inland moving  
 531 Indian monsoon depressions over Bay of Bengal. *SPIE Asia-Pacific Remote Sensing*, Remote  
 532 Sensing and Modeling of the Atmosphere, Oceans, and Interactions VI, 98820K, doi:10.1117/  
 533 12.2239712, URL <http://dx.doi.org/10.1117/12.2239712>.

534 Ramanathan, K. R., and K. P. Ramakrishnan, 1933: The Indian southwest monsoon and the struc-  
 535 ture of depressions associated with it. *Mem. Ind. Meteor. Dept.*, **26**, 13–36.

- 536 Rao, K. N., and S. Jayamaran, 1958: A statistical study of frequency of depressions and cyclones  
537 in the Bay of Bengal. *Indian J. Meteor. Geophys.*, **9**, 187–194.
- 538 Roy, P. S., and Coauthors, 2015: Development of decadal (1985–1995–2005) land use and land  
539 cover database for India. *Remote Sens.*, **7** (3), 2401–2430, doi:10.3390/rs70302401, URL <http://dx.doi.org/10.3390/rs70302401>.  
540
- 541 Shukla, J., 1978: CISK-barotropic-baroclinic instability and the growth of monsoon depressions.  
542 *J. Atmos. Sci.*, **35** (3), 495–508, doi:10.1175/1520-0469(1978)035<0495:CBBIAT>2.0.CO;2,  
543 URL [http://dx.doi.org/10.1175/1520-0469\(1978\)035<0495:CBBIAT>2.0.CO;2](http://dx.doi.org/10.1175/1520-0469(1978)035<0495:CBBIAT>2.0.CO;2).
- 544 Shutts, G., 2005: A kinetic energy backscatter algorithm for use in ensemble prediction systems.  
545 *Quart. J. Roy. Meteor. Soc.*, **131** (612), 3079–3102, doi:10.1256/qj.04.106, URL <http://dx.doi.org/10.1256/qj.04.106>.  
546
- 547 Van den Dool, H., J. Huang, and Y. Fan, 2003: Performance and analysis of the constructed ana-  
548 logue method applied to us soil moisture over 1981–2001. *J. Geophys. Res. Atmos.*, **108** (D16),  
549 doi:10.1029/2002JD003114, URL <http://dx.doi.org/10.1029/2002JD003114>.
- 550 Vinod Kumar, A., A. Chandrasekar, K. Alapaty, and D. Niyogi, 2007: The impact of assimi-  
551 lating soil moisture, surface temperature, and humidity and the traditional four dimensional  
552 data assimilation on the simulation of a monsoon depression over India using a mesoscale  
553 model. *J. Appl. Meteor. Climatol.*, **47**, 1393–1412, doi:10.1175/2007JAMC1599.1, URL <http://dx.doi.org/10.1175/2007JAMC1599.1>.  
554
- 555 Wagner, W., W. Dorigo, R. de Jeu, D. Fernandez, J. Benveniste, E. Haas, and M. Ertl, 2012:  
556 Fusion of active and passive microwave observations to create an essential climate vari-  
557 able data record on soil moisture. *Proceedings of the XXII International Society for Pho-*

558 *togrammetry and Remote Sensing (ISPRS) Congress, Melbourne, Australia*, Vol. 25, doi:  
559 10.5194/isprsannals-I-7-315-2012, URL <http://dx.doi.org/10.5194/isprsannals-I-7-315-2012>.

560 Walters, D., and Coauthors, 2015: The Met Office Unified Model Global Atmosphere 6.0/6.1  
561 configurations. *Geosci. Model Dev. Disc.*, doi:10.5194/gmd-2016-194, URL [http://dx.doi.org/](http://dx.doi.org/10.5194/gmd-2016-194)  
562 10.5194/gmd-2016-194, accepted.

563 Welch, B. L., 1947: The generalization of student's' problem when several different population  
564 variances are involved. *Biometrika*, **34** (1/2), 28–35, doi:10.2307/2332510, URL [http://www.](http://www.jstor.org/stable/2332510)  
565 [jstor.org/stable/2332510](http://www.jstor.org/stable/2332510).

566 Wilson, D. R., A. C. Bushell, A. M. Kerr-Munslow, J. D. Price, and C. J. Morcrette, 2008: PC2:  
567 A prognostic cloud fraction and condensation scheme. I: Scheme description. *Quart. J. Roy.*  
568 *Meteor. Soc.*, **134**, 2093–2107, doi:10.1002/qj.333, URL <http://dx.doi.org/10.1002/qj.333>.

569	<b>LIST OF FIGURES</b>	
570	<b>Fig. 1.</b>	Bowen ratio (lines) and precipitation (colours) for a 34-depression composite (1998-2014),
571		as described by Hunt et al. (2016a); the composite is normalised such that the centre of each
572		depression is placed at the origin, and each is rotated so that the heading is up the page. For
573		both fields, only points over land were composited. . . . . 31
574	<b>Fig. 2.</b>	Monthly soil moisture climatologies for the Indian peninsula from two products: a) NOAA
575		CPC reanalysis total soil moisture (data provided by the NOAA/OAR/ESRL PSD, Boulder,
576		Colorado, USA, from their website at <a href="http://www.esrl.noaa.gov/psd/">http://www.esrl.noaa.gov/psd/</a> ) and b) ESA
577		CCI satellite-derived volumetric soil moisture. . . . . 32
578	<b>Fig. 3.</b>	Average MD tracks for each month (June through September represented by red, blue, green,
579		and black respectively) during the Indian monsoon. Solid lines represent mean tracks from
580		the Hunt et al. (2016a) database, dashed lines from the Hurley and Boos (2015) database.
581		These tracks also include days where the disturbance is classified as a monsoon low, as well
582		as a monsoon depression. . . . . 33
583	<b>Fig. 4.</b>	Map showing the three masks used in the experiments in this study. The red box covers the
584		entire peninsula and some of the rest of South Asia, the green box approximates the region
585		where the monsoon trough is most active, and the orange box covers the intensely irrigated
586		and farmed area in the Himalayan foothills. . . . . 34
587	<b>Fig. 5.</b>	Track results from varying soil moisture in (a) the monsoon trough and (b) the sub-
588		Himalayan <i>arable zone</i> . For each sub-experiment, the average track is given by the thick
589		line with its termination given by the filled circles, and the individual ensemble 10-member
590		track terminations are given by crosses of the same colour. Also shown, in pale green, is
591		a concave hull of the “100%” (for (a), this is simply the control) ensemble plume for each
592		experiment. In (a), the official MD track from the Indian Meteorology Department is given
593		by the solid black line; in (b), the border of the <i>arable zone</i> is denoted by the dashed black
594		line. . . . . 35
595	<b>Fig. 6.</b>	Differences in selected fields of the composite mean ensembles for the 500% and 1% (the
596		former minus the latter) <i>trough zone</i> experiment. The composite is normalised such that its
597		centre lies at the origin, but no rotation is carried out; these are then presented as a height-
598		longitude cross section (at zero latitude). Greyed areas indicate the difference between the
599		sub-experiment composites was not met at the 95% significance level according to a 10,000
600		member bootstrap test. The selected fields are: (a) potential vorticity ( $10^{-7} \text{ K m}^2 \text{ kg}^{-1} \text{ s}^{-1}$ ),
601		(b) relative humidity (%), and (c) temperature (K). White lines on each subfigure indicate
602		the zero contour. . . . . 36
603	<b>Fig. 7.</b>	Longitude-latitude cross-sections of composite precipitation ( $\text{mm day}^{-1}$ ) and 850 hPa
604		winds, taken as the difference of the ensemble means for the 500% and 1% sub-experiments
605		(i.e. 500% mean minus 1% mean) of (a) the <i>trough zone</i> experiment and (b) the <i>arable zone</i>
606		experiment. Construction and representation of significance are identical to that of Fig. 6.
607		Note that while these composites are centred on the MD, they are not rotated. . . . . 37
608	<b>Fig. 8.</b>	Differences in selected fields of the composite mean ensembles for the 500% and 1% <i>arable</i>
609		<i>zone</i> experiment. Construction identical to Fig. 6, except that these are latitude-height cross-
610		sections. The selected fields are: (a) potential vorticity ( $10^{-7} \text{ K m}^2 \text{ kg}^{-1} \text{ s}^{-1}$ ), (b) relative
611		humidity (%), and (c) temperature (K). White lines on each subfigure indicate the zero con-
612		tour. . . . . 38

613 **Fig. 9.** Selected fields as a function of normalised depression lifetime for the trough experiment,  
 614 with the soil moisture changes coloured thus: 1% - red, 80% - yellow, 120% - green, 500%  
 615 - blue. From top to bottom, they are: the maximum CAPE ( $\text{J kg}^{-1}$ ) found in the advance  
 616 quadrant<sup>1</sup> of the MD; mean total precipitable water (mm); mean temperature anomaly (K)  
 617 between 850 and 400 hPa; and maximum relative vorticity ( $10^{-5}\text{s}^{-1}$ ). The thick, solid lines  
 618 represent the ensemble average, with the thinner, dashed lines representing the ensemble  
 619 minimum and maximum values. Each is computed over a box of side length 250 km centred  
 620 on the MD centre. . . . . 39



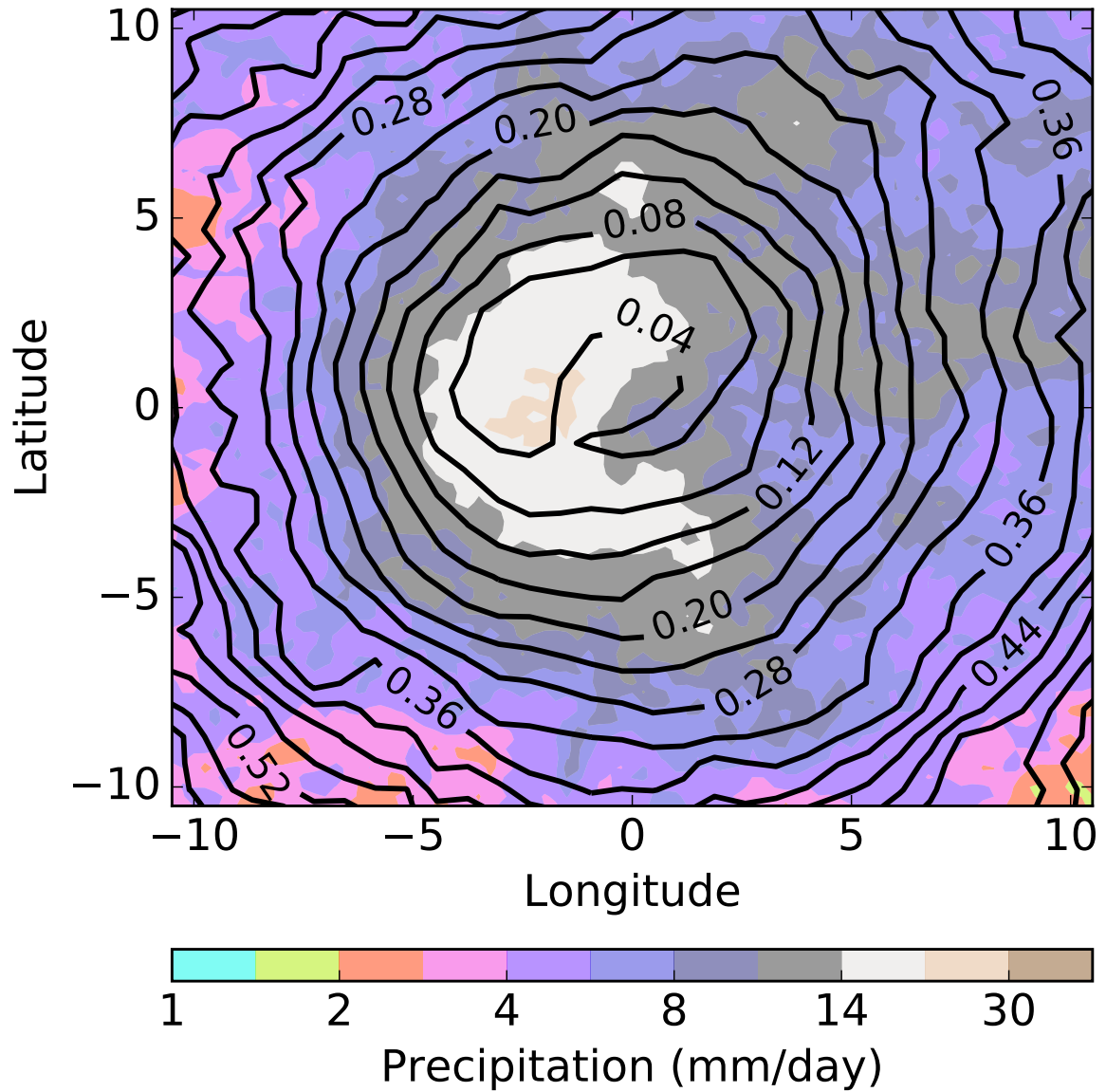


FIG. 1. Bowen ratio (lines) and precipitation (colours) for a 34-depression composite (1998-2014), as described by Hunt et al. (2016a); the composite is normalised such that the centre of each depression is placed at the origin, and each is rotated so that the heading is up the page. For both fields, only points over land were composited.

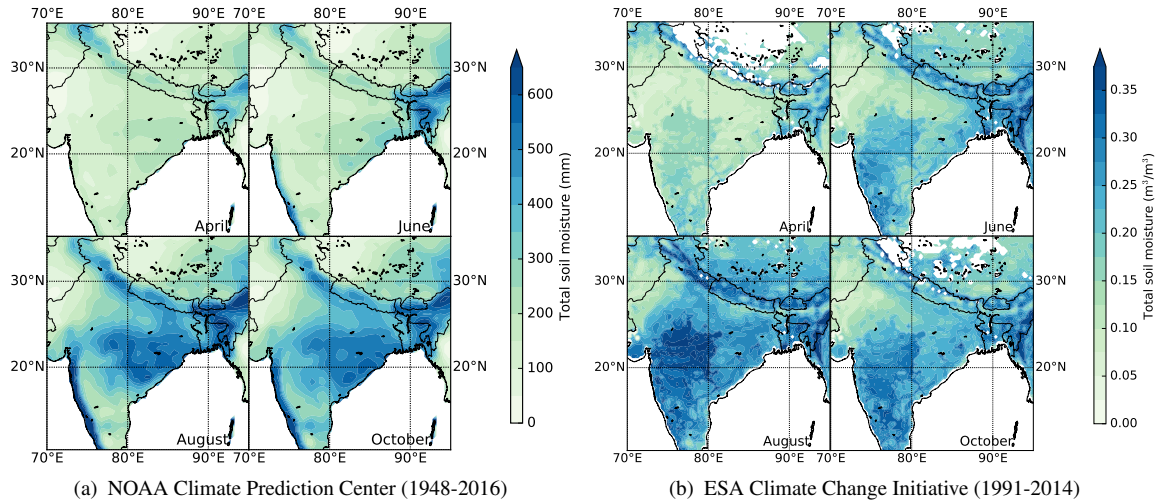


FIG. 2. Monthly soil moisture climatologies for the Indian peninsula from two products: a) NOAA CPC re-analysis total soil moisture (data provided by the NOAA/OAR/ESRL PSD, Boulder, Colorado, USA, from their website at <http://www.esrl.noaa.gov/psd/>) and b) ESA CCI satellite-derived volumetric soil moisture.

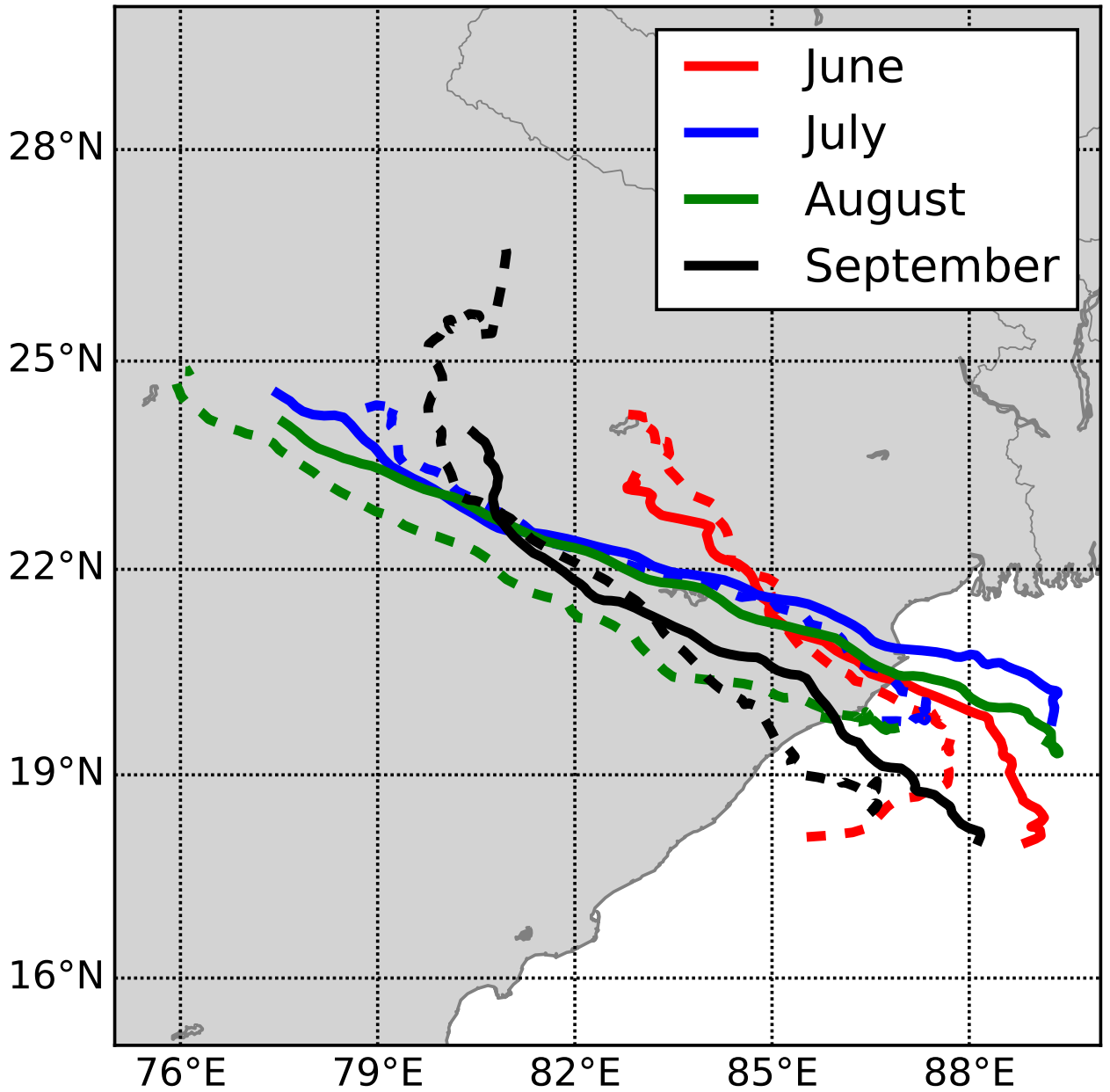


FIG. 3. Average MD tracks for each month (June through September represented by red, blue, green, and black respectively) during the Indian monsoon. Solid lines represent mean tracks from the Hunt et al. (2016a) database, dashed lines from the Hurley and Boos (2015) database. These tracks also include days where the disturbance is classified as a monsoon low, as well as a monsoon depression.

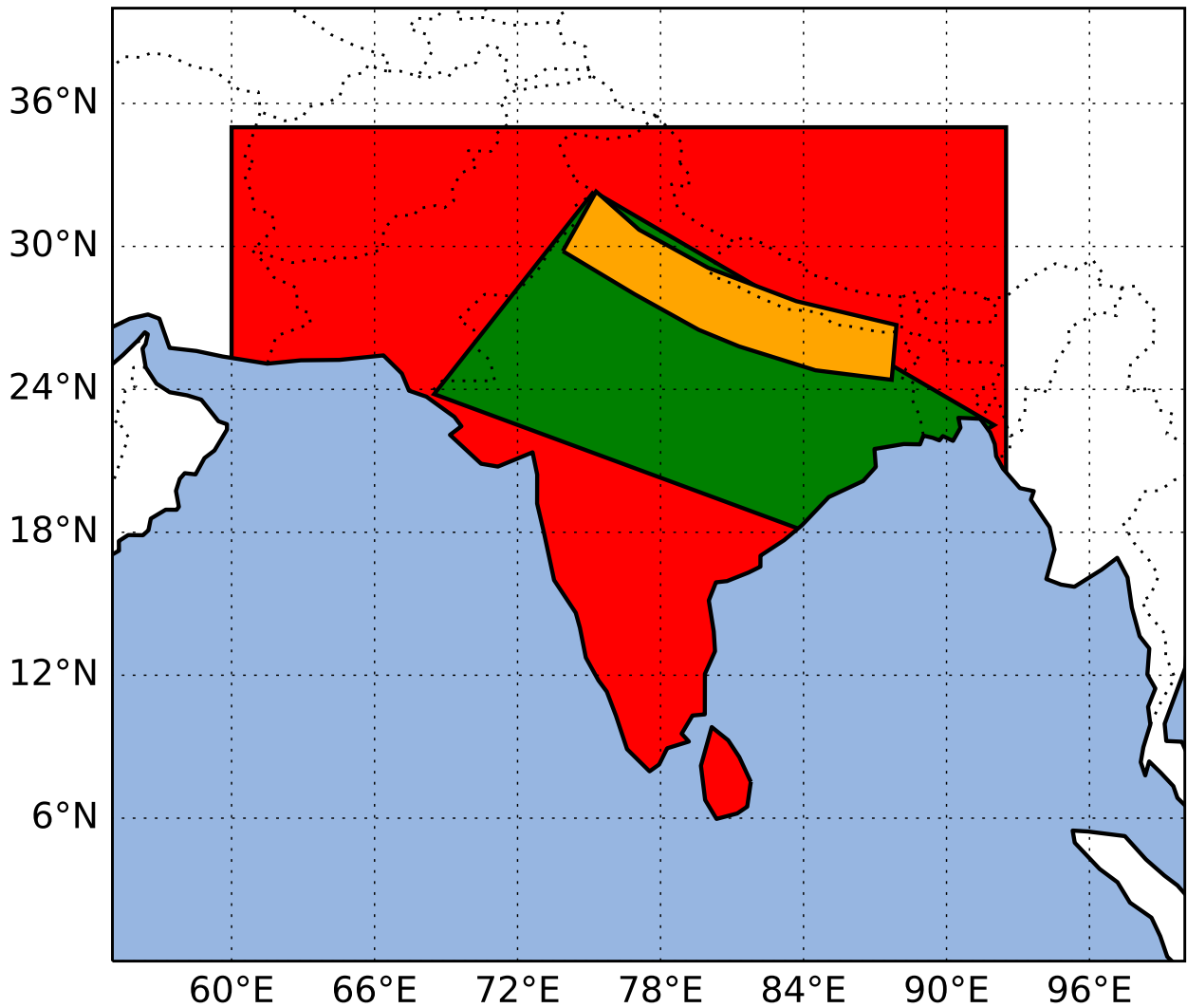


FIG. 4. Map showing the three masks used in the experiments in this study. The red box covers the entire peninsula and some of the rest of South Asia, the green box approximates the region where the monsoon trough is most active, and the orange box covers the intensively irrigated and farmed area in the Himalayan foothills.

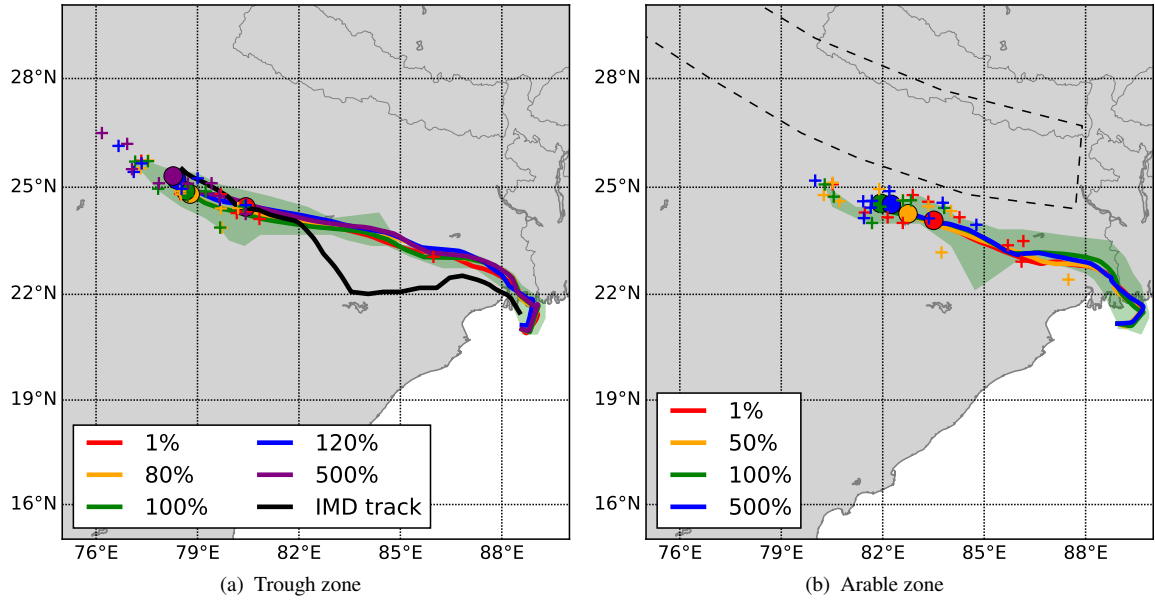


FIG. 5. Track results from varying soil moisture in (a) the monsoon trough and (b) the sub-Himalayan *arable zone*. For each sub-experiment, the average track is given by the thick line with its termination given by the filled circles, and the individual ensemble 10-member track terminations are given by crosses of the same colour. Also shown, in pale green, is a concave hull of the “100%” (for (a), this is simply the control) ensemble plume for each experiment. In (a), the official MD track from the Indian Meteorology Department is given by the solid black line; in (b), the border of the *arable zone* is denoted by the dashed black line.

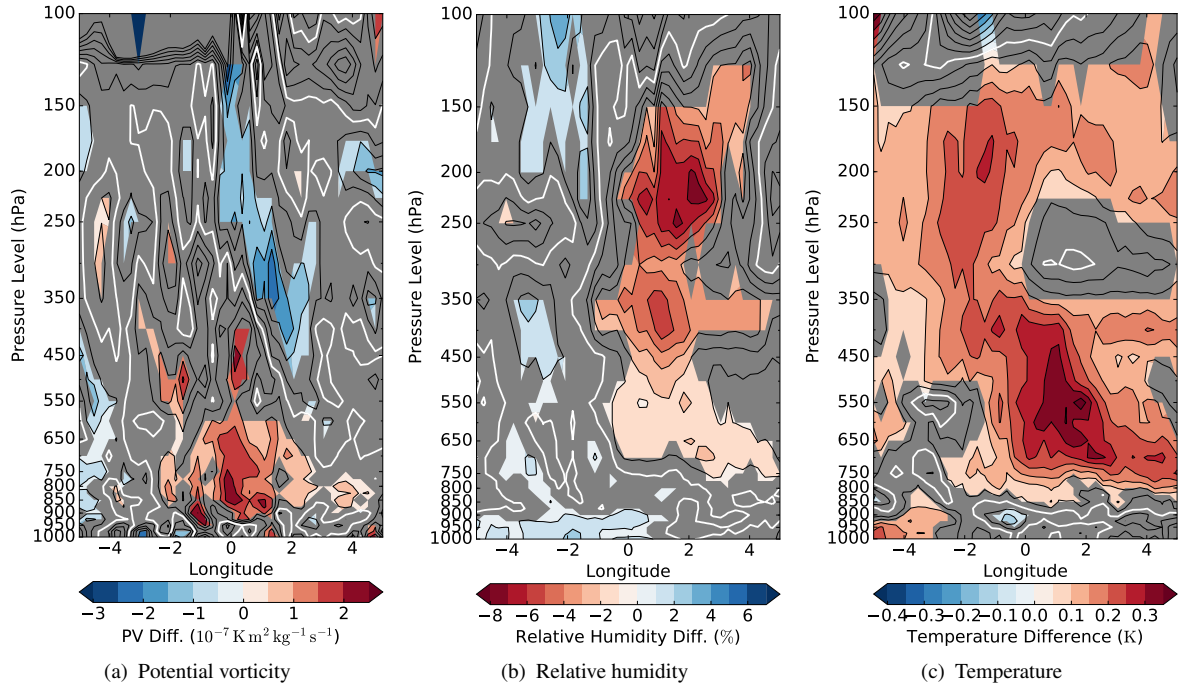


FIG. 6. Differences in selected fields of the composite mean ensembles for the 500% and 1% (the former minus the latter) *trough zone* experiment. The composite is normalised such that its centre lies at the origin, but no rotation is carried out; these are then presented as a height-longitude cross section (at zero latitude). Greyed areas indicate the difference between the sub-experiment composites was not met at the 95% significance level according to a 10,000 member bootstrap test. The selected fields are: (a) potential vorticity ( $10^{-7} \text{ K m}^2 \text{ kg}^{-1} \text{ s}^{-1}$ ), (b) relative humidity (%), and (c) temperature (K). White lines on each subfigure indicate the zero contour.

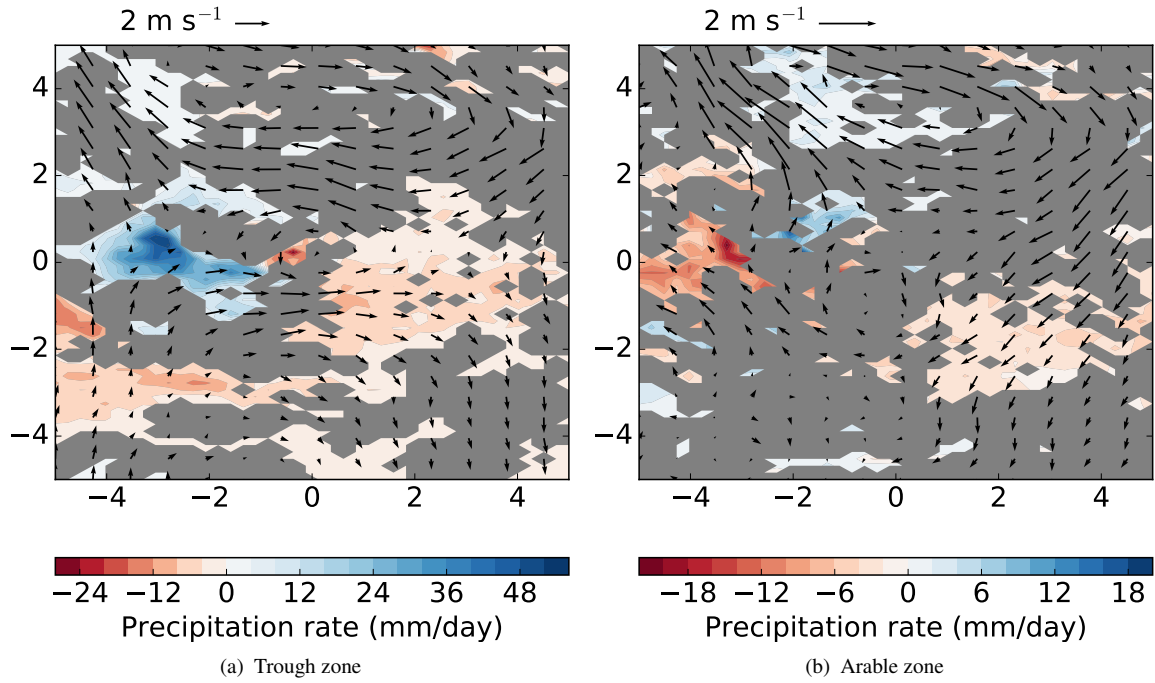


FIG. 7. Longitude-latitude cross-sections of composite precipitation ( $\text{mm day}^{-1}$ ) and 850 hPa winds, taken as the difference of the ensemble means for the 500% and 1% sub-experiments (i.e. 500% mean minus 1% mean) of (a) the *trough zone* experiment and (b) the *arable zone* experiment. Construction and representation of significance are identical to that of Fig. 6. Note that while these composites are centred on the MD, they are not rotated.

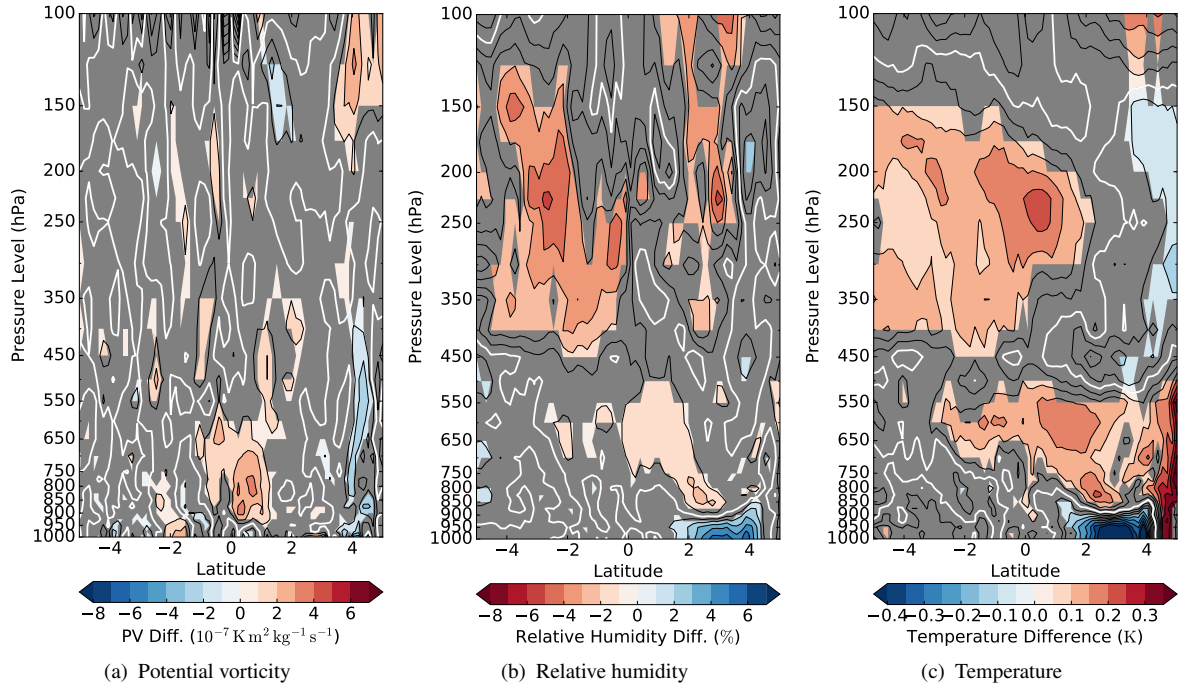


FIG. 8. Differences in selected fields of the composite mean ensembles for the 500% and 1% *arable zone* experiment. Construction identical to Fig. 6, except that these are latitude-height cross-sections. The selected fields are: (a) potential vorticity ( $10^{-7} \text{ K m}^2 \text{ kg}^{-1} \text{ s}^{-1}$ ), (b) relative humidity (%), and (c) temperature (K). White lines on each subfigure indicate the zero contour.



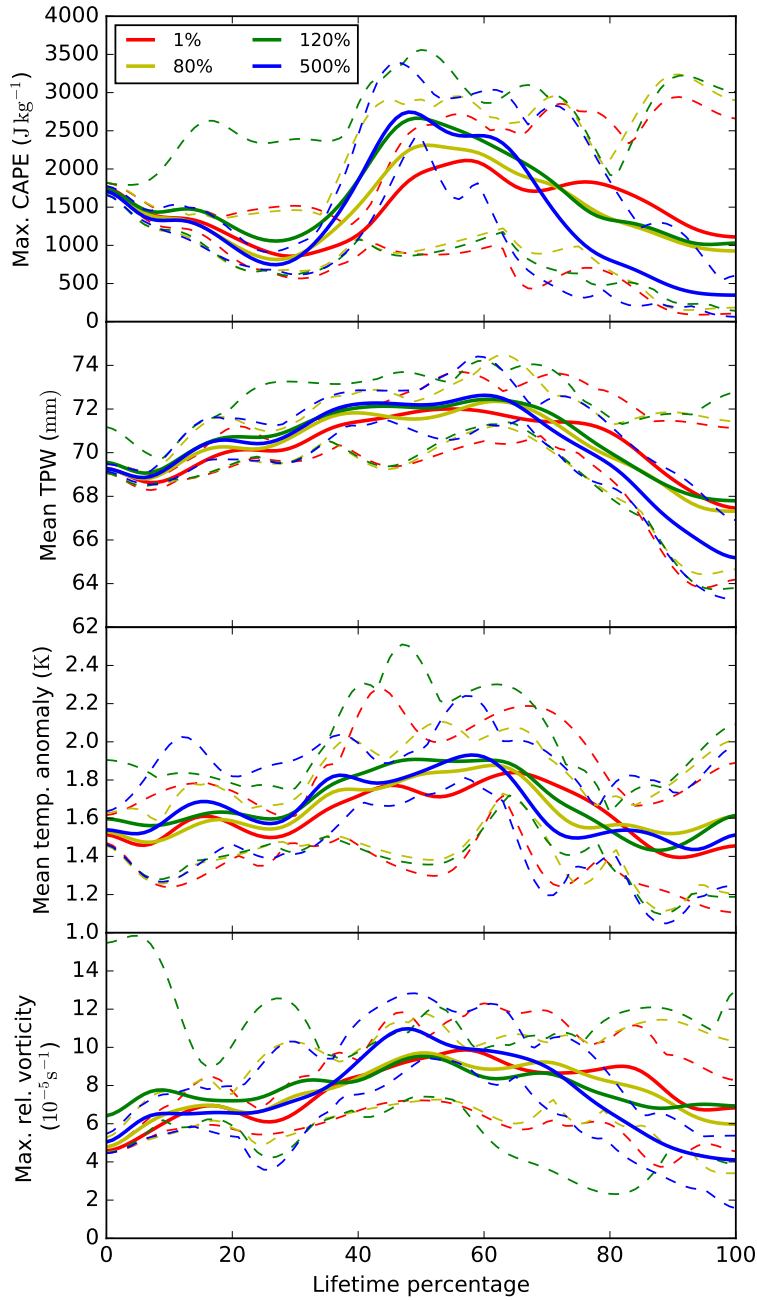


FIG. 9. Selected fields as a function of normalised depression lifetime for the trough experiment, with the soil moisture changes coloured thus: 1% - red, 80% - yellow, 120% - green, 500% - blue. From top to bottom, they are: the maximum CAPE ( $\text{J kg}^{-1}$ ) found in the advance quadrant<sup>4</sup> of the MD; mean total precipitable water (mm); mean temperature anomaly (K) between 850 and 400 hPa; and maximum relative vorticity ( $10^{-5} \text{s}^{-1}$ ). The thick, solid lines represent the ensemble average, with the thinner, dashed lines representing the ensemble minimum and maximum values. Each is computed over a box of side length 250 km centred on the MD centre.